Journal of proteome research

pubs.acs.org/jpr

Article

Data-Independent Acquisition Proteomics and N-Terminomics Methods Reveal Alterations in Mitochondrial Function and Metabolism in Ischemic-Reperfused Hearts

Published as part of Journal of Proteome Research virtual special issue "Canadian Proteomics".

Bridgette Hartley, Wesam Bassiouni, Andrej Roczkowsky, Richard Fahlman, Richard Schulz,* and Olivier Julien*

Cite This: *J. Proteome Res.* 2024, 23, 844−856

Read Online

ACCESS | Metrics & More | Article Recommendations | Supporting Information

ABSTRACT: Myocardial ischemia-reperfusion (IR) (stunning) injury triggers changes in the proteome and degradome of the heart. Here, we utilize quantitative proteomics and comprehensive degradomics to investigate the molecular mechanisms of IR injury in isolated rat hearts. The control group underwent aerobic perfusion, while the IR injury group underwent 20 min of ischemia and 30 min of reperfusion to induce a stunning injury. As MMP-2 activation has been shown to contribute to myocardial injury, hearts also underwent IR injury with ARP-100, an MMP-2-preferring inhibitor, to dissect the contribution of MMP-2 to IR injury. Using data-independent acquisition (DIA) and mass spectroscopy, we quantified 4468 proteins in ventricular extracts, whereby 447 proteins showed significant alterations among the three groups. We then used subtiligase-mediated N-terminomic labeling to identify more than a hundred specific cleavage sites. Among these protease substrates, 15 were identified following IR injury. We identified alterations in numerous proteins involved in mitochondrial function and metabolism following IR injury. Our findings provide valuable insights into the biochemical mechanisms of myocardial IR injury, suggesting alterations in reactive oxygen/nitrogen species handling and generation, fatty acid metabolism, mitochondrial function and metabolism, and cardiomyocyte contraction.

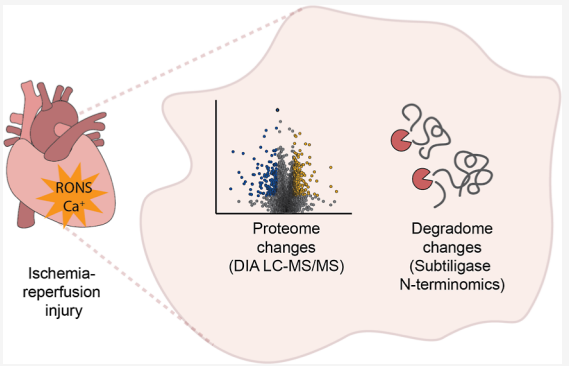

KEYWORDS: *proteolysis, ischemic heart disease, intracellular protease, matrix metalloproteinase, degradomics, mass spectrometry, data-independent acquisition*

INTRODUCTION

Cardiovascular diseases caused 19.1 million deaths globally in 2020.[1] Ischemic heart disease results from partial or total coronary artery occlusion, often due to atherosclerotic plaque buildup, coronary vasospasm, or blood clots.[2] To prevent ischemic cell death and preserve cardiac function, reperfusion by pharmacological or mechanical intervention is necessary.[3] However, reperfusion can cause further damage to cardiac cells, due to the cellular changes in response to oxidative stress, also known as ischemia-reperfusion (IR) injury.[3−6]

Previous proteomics studies have reported protein abundance changes following myocardial IR injury, using 2D-gel electrophoresis[7−9] or using in-solution digestion and isobaric labeling[10] followed by liquid chromatography and tandem mass spectrometry (LC−MS/MS).[7−9] In recent years, major advances in protein identification and quantification have been enabled by an increase in the speed and sensitivity of mass spectrometers, improved sample preparation, and the development of data-independent acquisition (DIA) methods which continuously monitor peptide abundances.[11−14] DIA improves the quantification of low abundant peptides,[11] improves reproducibility in complex samples,[12,14] and enables deep proteome coverage without the use of extensive prefractionation techniques.[13] The utilization of these newer technologies to assess protein abundance changes following myocardial IR injury has not yet been reported.

Intracellular proteins cleaved by various proteases during myocardial IR injury, including cardiac troponin I,[15−19] cardiac troponin T,[20,21] titin,[22] myosin light chain 1,[9] sarco/endoplasmic reticulum calcium ATPase (SERCA2a),[23,24] α-actinin,[20,21,25,26] ryanodine receptor,[24] lactate dehydrogenase (LDH),[19] and tropomyosin,[21] among others, have been

Received: November 11, 2023
Revised: January 6, 2024
Accepted: January 10, 2024
Published: January 24, 2024

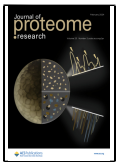

identified using biochemical and imaging techniques. Specific cleavage sites, and the protease(s) responsible for their proteolysis, remain largely unknown, although calpains, cathepsins, caspases, and matrix metalloproteinases (MMPs),[27] such as MMP-2, have been identified on the basis of pharmacological inhibition and transgenic approaches.[28]

Degradomics is the study of proteases, their substrates, and inhibitors. Traditional studies of proteolysis in biological systems include immunoblotting, immunohistochemistry, and immunofluorescence. However, these processes have low throughput and rely on the quality, availability, and specificity of antibodies to the substrate protein of interest. Developing high-throughput methods to identify proteolytic cleavage sites can lead to a better understanding of the progression of IR injury. Subtiligase-mediated N-terminomics, for example, enables the identification of hundreds of cellular proteolytic cleavage events.[29−31]

Here, we aimed to assess the intracellular proteome and degradome changes following myocardial IR injury in isolated, perfused rat hearts. We used mass spectrometry approaches with DIA analysis to assess the global proteome changes. In addition, we used subtiligase-mediated N-terminomics to identify protease cleavage sites in these hearts and expand the repertoire of known proteins cleaved during IR injury. Using direct DIA, we quantified 4468 proteins and found statistically significant alterations in 447. Using subtiligase-based N-terminomics, we identified 132 to 149 cleavage sites in each heart group, with 15 unique to hearts that were subjected to IR injury. In particular, our data indicate alterations in mitochondrial function and metabolism, suggesting potential therapeutic targets to limit damage due to IR.

EXPERIMENTAL PROCEDURES

Animal experiments in this study were approved by the University of Alberta Institutional Animal Care and Use Committee (AUP 329). All animals used in this study were treated in accordance with the Guide to the Care and use of experimental animals by the Canadian Council on Animal Care (CCAC) and the Guide for the Care and Use of Laboratory Animals published by the United States National Institutes of Health (NIH, eighth edition, revised 2011).

Isolated Working Heart Perfusions

Adult male rat hearts were isolated and perfused as working rat hearts, as described previously.[23] Briefly, male Sprague−Dawley rats (300−400 g) were anesthetized with sodium pentobarbital (240 mg/kg), and hearts were rapidly excised and rinsed in ice-cold (4 °C) Krebs-Henseleit solution. Hearts were initially perfused in the Langendorff mode for 10 min at a constant pressure of 60 mmHg at 37 °C. Then, hearts were switched to the working heart mode.

Control hearts (AER) were perfused aerobically for 70 min. Ischemia-reperfused hearts were perfused aerobically for 20 min, followed by 20 min of global, no-flow ischemia, and 30 min of aerobic reperfusion. Either vehicle (0.05% DMSO) or the MMP-2 preferring inhibitor, ARP-100 (10 μM), were added 10 min prior to the onset of ischemia. Following perfusion, all hearts were flash frozen in liquid nitrogen and stored at −80 °C until use. Extensive physiological data on heart function are found in ref 23. A detailed protocol is provided in the Supporting Information. Six hearts were perfused into each group. Due to tissue availability and material use, five hearts from each group were used for proteomics and two for degradomics.

Preparation of Ventricular Extracts after Perfusion

Pulverized frozen ventricles were lysed in RIPA buffer (Thermo Fisher Scientific) supplemented with 5% (w/v) SDS in the presence of protease inhibitors [5 mM EDTA, 1 mM 4-(2-aminoethyl) benzenesulfonyl fluoride hydrochloride, 1 mM phenylmethanesulfonyl fluoride, and 4 mM iodoacetamide] using a mortar and pestle on ice (4 °C). The lysates were then homogenized by sonication using a Qsonica sonicator (Mandel Inc.) for 2 min (40% amplitude, 2 s on, 2 s off) on ice (4 °C). Total protein concentration was assessed by the bicinchoninic acid (BCA) assay using bovine serum albumin (Bio-Rad Inc.) as a standard.

Sample Preparation Using Suspension-Trapping (S-Trap Columns) for Label-Free Protein Quantification

Ventricular extracts (50 μg of total protein/sample) from five biological replicates (hearts) per condition were acidified with phosphoric acid to 1.2% (v/v) at room temperature. Acidified proteins were captured on S-trap columns (ProtiFi). The columns were washed four times with 90% methanol in 100 mM tetraethylammonium bicarbonate to remove detergent and other contaminants. Trypsin was suspended in 50 mM tetraethylammonium bicarbonate and added to the columns (1:10 μg total protein/μg trypsin, mass-spectrometry grade trypsin, Promega Inc.). The columns were incubated overnight at 37 °C. The tryptic peptides were eluted in one fraction with 0.2% formic acid followed by 50% acetonitrile. The samples were dried under a vacuum to remove excess acetonitrile. Once dried, peptides were resuspended in 50 μL of 0.1% trifluoroacetic acid and desalted on C-18 resin at room temperature (ZipTip, Millipore Sigma). The samples were then dried again and resuspended in 20 μL of 0.1% formic acid for analysis on LC−MS/MS.

Mass Spectrometry for Proteome Quantification (Proteomics Workflow)

LC−MS/MS was carried out by reverse phase LC (Thermo Scientific EASY-nLC 1200) interfaced to an Orbitrap Fusion Lumos Tribrid (Thermo Fisher Scientific) mass spectrometer. An analytical column (1.7 μm beads, 120 Å pore size, 75 μm × 25 cm, Aurora; IonOpticks) was used for the reverse-phase separation of the peptide mixture. Peptides were eluted over a linear gradient over the course of 120 min from 3.85 to 36.8% acetonitrile in 0.1% formic acid. Spectra were acquired using DIA with an MS1 orbitrap resolution of 120,000 fwhm and a scan range of 350−2000 m/z. MS2 resolution was 30,000 fwhm with a scan range of 350−1400 m/z and an isolation window of 38.5 m/z. The positive ion voltage was 1650 V by using higher-energy collision dissociation (HCD). The dynamic exclusion properties include exclusion after one time for 45 s.

Raw data were analyzed using Spectronaut (v18) software against the rat proteome (2023.05.10. rat proteome sequence downloaded from https://www.uniprot.org/). Search parameters include a parent mass tolerance of 15 ppm, a fragment ion mass tolerance of 0.8 Da, up to two missed trypsin cleavages, and charge states of 2−4. Constant modification was set to carbamidomethylation of cysteine, and variable modifications include oxidation of methionines and acetylated protein N-termini. Identified peptides were searched against a random

https://doi.org/10.1021/acs.jproteome.3c00754
J. Proteome Res. 2024, 23, 844−856

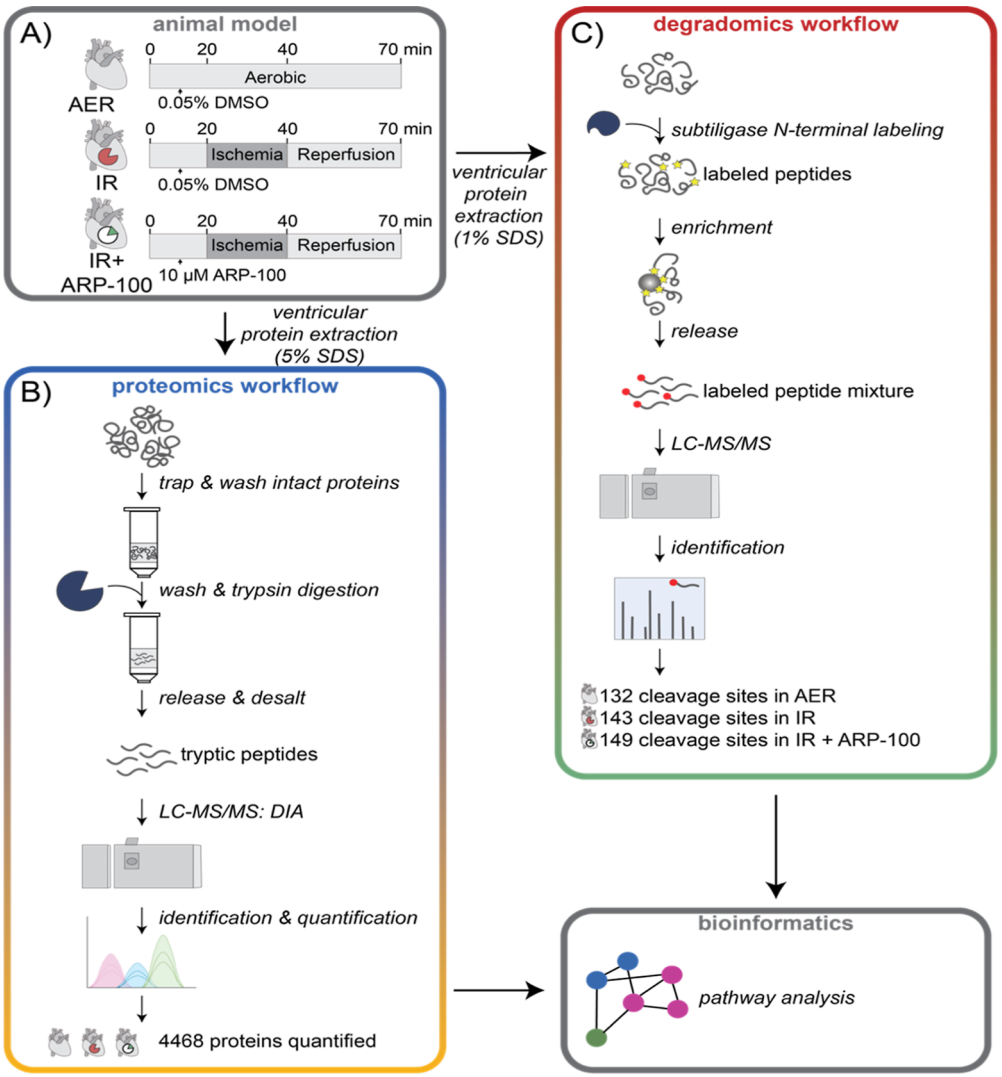

Figure 1. Overview of mass spectrometry-based proteomics and degradomics used to investigate ventricular extracts from isolated perfused hearts. (A) Three heart groups include aerobically perfused for 70 min with 0.05% DMSO vehicle (AER); hearts perfused aerobically for 20 min followed by 20 min of global no-flow ischemia and 30 min of aerobic reperfusion (IR); as IR but with 10 μM ARP-100 (IR + ARP-100). AER is represented by a gray heart, IR by a gray heart with a red protease, and IR + ARP-100 with a white protease and green inhibitor. (B) Quantitative proteomics is used to quantify proteome changes in ventricular extracts following IR injury. Proteins are extracted (5% SDS buffer) from heart tissue, followed by capture on S-trap columns, trypsin digestion, and extraction. Tryptic peptides are identified and quantified using data-independent acquisition (DIA) on LC−MS/MS. Degradomics is used to identify protease substrates cleaved in the three heart groups. (C) Ventricular extracts (1% SDS buffer) from all groups were subjected to N-terminal labeling. The enzyme subtiligase ligates a biotinylated peptide ester to the N-termini of the proteolytic fragments. Labeled protein fragments are enriched on neutravidin beads, digested with trypsin, and released. Labeled peptides contain a unique mass at the N-terminal (red, aminobutyric acid, +154 Da) to enable the identification of the protease substrates and the precise cleavage site locations originating from proteolysis in the heart. Tryptic peptides are identified using LC−MS/MS.

decoy protein database to evaluate the false-positive rate (set to 1%). All raw data are deposited in MassIVE (MSV000092906). Gene ontology was performed using https://metascape.org against the rat proteome. Enrichment was performed using GO biological processes, KEGG pathway, Reactome Gene Sets, CORUM, TRRUST, PaGenBase, and Wiki Pathways.[32]

Hypothesis testing for heatmaps was performed using Analysis of Variance (ANOVA) followed by the Tukey honest significant difference post hoc test. Protein abundances between samples were normalized using a z-score. Heatmaps were constructed using R (R Core Team 2018, v4.2.1) with superheat.[33] Gene ontology was performed on proteins with significant changes in abundance (FC > 2 and $p < 0.05$) using https://metascape.org against the rat proteome.[32] A detailed protocol is provided in the Supporting Information.

N-Terminomic Labeling (Degradomics Workflow)

N-terminal labeling was performed on lysates with 1 μM subtiligase (wild-type and M222A mutant) and 1 mM TEVest6 for 2 h at room temperature. Samples were taken at 1 h for Western blot analysis to test the efficiency of labeling (data not shown). Labeled proteins were precipitated in ice-cold acetonitrile overnight (−80 °C) followed by centrifugation at 14,000g for 30 min. Pellets were dried at room temperature and denatured in 8 M guanidine hydrochloride. Proteins were then reduced with 2 mM tris(2-carboxyethyl) phosphine and alkylated in 4 mM iodoacetamide. The remaining iodoacetamide was quenched with 10 mM

https://doi.org/10.1021/acs.jproteome.3c00754
J. Proteome Res. 2024, 23, 844−856

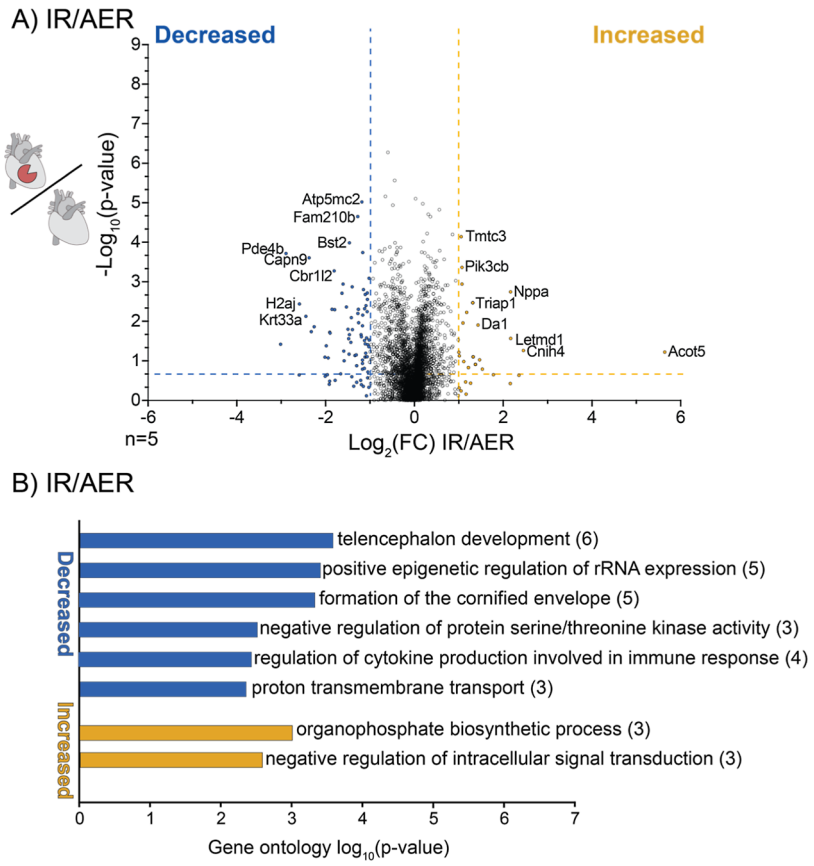

Figure 2. Relative proteome changes in ventricular extracts following ischemia-reperfusion (IR) injury compared with aerobic controls (AER). (A) Volcano plot shows proteins with a decreased (blue) or increased (orange) abundance in IR compared to aerobic control hearts with a fold change greater than two and a significant *p*-value of <0.05. Proteins are identified with the gene name for simplicity. AER is represented by a gray heart and IR by a gray heart with a red protease. (B) Bar graph presented shows the enriched gene ontology pathways corresponding to protein abundances significantly altered (decreased in blue or increased in yellow) by two-fold with a *p*-value <0.05. A detailed list of proteins is provided in Supporting Information 3 and 4. Five biological replicates for each group were analyzed.

dithiothreitol, and the proteins were precipitated in ice-cold ethanol for 48 h (−20 °C). Biotinylated N-terminal peptides were captured on a neutravidin (Pierce High Capacity Neutravidin Agarose) resin for 18 h at room temperature. The resin was washed with 4 M guanidine hydrochloride, and protein fragments were trypsinized in 100 mM bicine at room temperature. Labeled peptides were released from the beads with tobacco etch virus protease (purified in our laboratory) overnight at room temperature. The samples were dried, resuspended in 2.5% trifluoroacetic acid, desalted on C18 zip tips, and eluted with 80% acetonitrile and 0.1% trifluoroacetic acid. Peptides were dried under vacuum and resuspended in 15 μL of 0.1% formic acid for analysis on LC−MS/MS.

Mass Spectrometry for N-Terminomic Labeling

Peptides were separated using nanoflow-HPLC (Thermo Scientific EASY-nLC 1200) interfaced to an Orbitrap Fusion Lumos Tribrid (Thermo Fisher Scientific) mass spectrometer. An analytical column (2 μm beads, 100 Å pore size, 75 μm × 25 cm, EASY-Spray; Thermo Fisher Scientific) was used for the reverse-phase separation of the peptide mixture. Peptides were eluted over a linear gradient over the course of 120 min from 3.85 to 36.8% acetonitrile in 0.1% formic acid. Spectra were acquired using data-dependent acquisition with an MS1 orbitrap resolution of 120,000 fwhm and a scan range of 375−1700 m/z. Charges between 2 and 7 were included. The positive ion voltage was 2100 V using HCD. The dynamic exclusion properties include exclusion after one time for 45 s.

Raw data were analyzed using Thermo Proteome Prospector (v 5. 22. 1) software against the rat proteome (2021.06.21. rat proteome sequence downloaded from https://www.uniprot.org/). Search parameters include a parent mass tolerance of 15 ppm, a fragment ion mass tolerance of 0.8 Da, up to three missed trypsin cleavages, charge states of 2, 3, 4, a constant mode of carbamidomethylation of cysteine, tryptic digestion, variable modifications of aminobutyric acid on protein N-termini, and oxidation of methionines. Identified peptides were searched against a random decoy protein database to evaluate the false-positive rate (set to 1%). All raw data are deposited in MassIVE (MSV000092906). Gene ontology was performed using https://metascape.org against the rat proteome. Enrichment was performed using GO biological processes, KEGG pathway, Reactome Gene Sets, CORUM, TRRUST, PaGenBase, and Wiki Pathways.[32]

Immunoblotting Analysis

Heart extracts were thawed on ice, and 20 μg of total protein of each sample was separated using SDS-polyacrylamide gel electrophoresis (4−20% gradient, Biorad 456−1086). Proteins were then wet-transferred to a nitrocellulose membrane using wet transfer (1.25 h at 35 V). Membranes were incubated at room temperature for 1.5 h with shaking in blocking buffer (LI-COR Biosciences), followed by overnight incubation with

https://doi.org/10.1021/acs.jproteome.3c00754
J. Proteome Res. 2024, 23, 844−856

the following primary antibody solutions at 4 °C: CH60 [Proteintech, (15282−1-AP); 1:1000], KAD1 [Proteintech, (14978−1-AP); 1:1000], MYL4 [Proteintech, (67533−1-Ig); 1:500], lactate dehydrogenase A (LDHA) [Proteintech, (21799−1-AP); 1:500], actinin alpha 2 (ACTN2) [Proteintech, (14221−1-AP); 1:1000], SERPH [Proteintech, (67863−1-Ig); 1:1000], beta-tubulin [Sigma-Aldrich, (T5293); 1:1000], alpha-tubulin [Abcam, (18251); 1:1000], and beta-actin [abcam, (18226); 1:1000]. Following that, membranes were incubated with goat antirabbit IgG secondary antibody [IRDye Li-Cor Biosciences (926−32210); 1:6000] for CH60, KAD1, and ACTN2, and goat antimouse IgG secondary antibody [IRDye Li-Cor Biosciences, (926−32210); 1:6000] for all other proteins, for 1 h at room temperature and imaged and quantified using LI-COR Odyssey XF imaging system and image studio.

RESULTS

Identification of Proteome Changes Resulting from Cardiac IR Injury

We used adult rat hearts that were isolated and perfused in the working heart mode as a model of IR injury. This method involves perfusing hearts in an oxygenated salt solution to mimic physiological conditions. We used three experimental groups: an aerobic control (AER) consisting of hearts continuously perfused for 70 min as a time control, an IR group consisting of hearts subjected to no-flow ischemia for 20 min followed by 30 min of reperfusion, and a treatment group (IR + ARP-100) consisting of hearts undergoing IR but treated with the MMP-2 preferring inhibitor, ARP-100 (Figure 1A).[23,34,35] Physiological data, including heart rate, cardiac output, and cardiac work before and after IR, have been previously reported[23] and are presented in Figure S1. In short, IR caused a decrease in the heart rate, cardiac output, and cardiac work. All were increased in the IR + ARP-100 group.

Ventricular proteins were extracted from each of $n = 5$ hearts per group for analysis by DIA LC−MS/MS, where we report the quantification of 4468 proteins (Figure 1B). Our results show that we successfully solubilized proteins from various cellular compartments, including the cytoplasm (16.4%), mitochondria (12.0%), nucleus (11.9%), and membrane bound (20.1%), identified by gene ontology analysis (Figure S2A). We identified between 4449 and 4465 proteins in each lysate with 4439 proteins common to all three heart groups. The strong overlap is reflected in the Venn diagram by a small area for proteins unique to each group (Figure S2B). Several vital structural proteins typically found in cardiac tissues (β-actin, α-tubulin, and β-tubulin) showed nonsignificant protein abundance changes, as expected, and acted as internal controls (Supporting Information 1 and 2).

We first performed a comparative analysis of protein abundance levels following IR injury compared with AER (Figure 2A). Using an unpaired Student's t test (p-value <0.05 and a fold change ≥2), we found 83 proteins decreased and 26 increased in abundance after IR injury. Proteins may increase in response to stress to prevent or even worsen cellular injury or undergo subcellular localization changes. We performed a gene ontology analysis and found that proteins with decreased abundance were involved in telencephalon development, positive epigenetic regulation of rRNA expression, cornified envelope formation, and proton transmembrane transport. Of note, cardiomyocyte proteins are typically not involved in telencephalon development and cornified envelope formation; thus, enrichment of these pathways could be due to processes occurring in noncardiomyocyte cells of the heart or be simply part of the inherent limitations of gene ontology analysis. Interestingly, we recently showed that MMP-2 localized to nucleoli regulates rRNA transcription by proteolysis of histones.[36] For example, the level of Na^+/K^+- transporting ATPase subunit alpha-3 (ATP1A3) (included in proton transmembrane transport) decreased by a fold change of 2 following IR injury. ATP1A3 is responsible for the transport of sodium out and potassium into the cytoplasm. Our findings are consistent with a previous in vitro study for IR injury which reported lower levels of ATP1A3 at the cell surface.[37]

Of the 26 proteins showing an increased protein level, we found that proteins involved in the organophosphate biosynthetic process and negative regulation of intracellular signal transduction were enriched (Figure 2B). For example, the abundance of natriuretic peptide A, involved in both pathways, was increased by a fold change of 4.5. The role of natriuretic peptides in cardiovascular diseases is well studied. For example, treatment with a synthetic alpha-human atrial natriuretic peptide before IR injury reduced infarct size, indicating a potential cardioprotective effect.[38] Although we observed an increase in the level of natriuretic peptide A, its cardioprotective effects remain unknown in the present study.

We also assessed ventricular protein abundance changes resulting from ARP-100 treatment during IR. We compared protein abundance levels in rat hearts following IR injury ± ARP-100 (Figure S3A). Using the same unpaired Student's t test (p-value <0.05 and a fold change ≥2), we found that 72 proteins decreased, and 42 increased in abundance in IR + ARP-100 hearts. The gene ontology analysis revealed that proteins with decreased abundance were involved in establishing protein localization to organelles, positive regulation of transmembrane transport, and cellular homeostasis (Figure S4A). Interestingly, phospholemman levels decreased in IR + ARP-100 hearts by a fold change of 2.4. Phospholemman associates with the Na/K^+-transporting ATPase,[39] and overexpression of a mutant lacking a phosphorylation site improved cardiac contractile function following IR injury.[40] These results uncover a potential mechanism for improving cardiac contractile function following ARP-100 treatment during IR injury. As a control, a comparative analysis of protein abundance changes in IR + ARP-100 compared to AER is presented (Figure S3B) with the gene ontology (Figure S4B). A complete list of the comparative and gene ontology analyses is provided in Supporting Information 4 and 5.

Overall Proteome Changes between AER, IR, and IR + ARP-100

Next, we aimed to assess the overall proteome changes among the three heart groups. We conducted ANOVA using a p-value threshold of 0.05, to determine which proteins significantly changed in abundance across the three groups. We then scaled the abundances (z-scores) to show the relative changes. The data are presented as a heatmap with hierarchical clustering based on the protein abundance patterns. We identified 447 proteins that exhibited significant changes in abundance, as illustrated in Figure 3A. The heatmap displays the changes as a result of IR injury by comparing column 1 (AER) and 2 (IR). The third column (IR + ARP-100) shows the pharmacoproteomic effects of an MMP-2 preferring inhibitor. We also

https://doi.org/10.1021/acs.jproteome.3c00754
J. Proteome Res. 2024, 23, 844−856

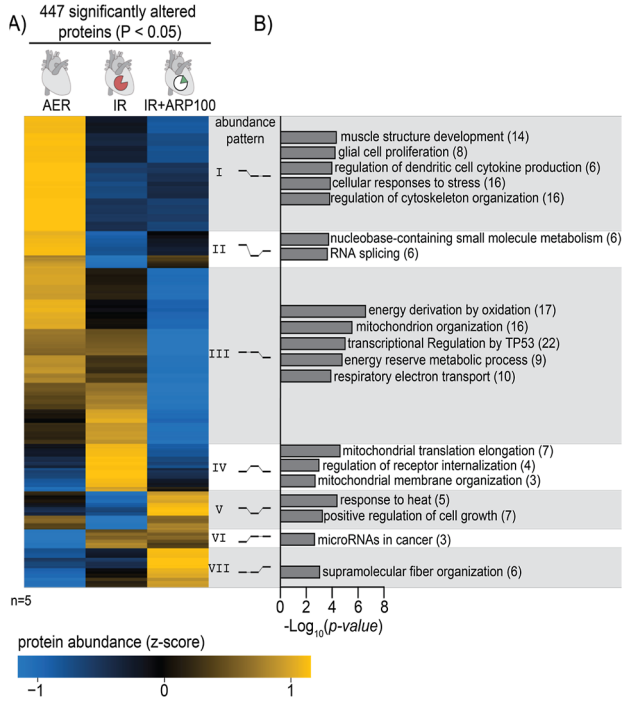

Figure 3. Significantly altered proteins quantified in ventricular extracts from AER, IR, and IR + ARP-100 heart groups using the proteomics workflow. Distinct protein abundance patterns between the heart groups are depicted as a heatmap. AER is represented by a gray heart, IR by a gray heart with a red protease, and IR + ARP-100 with a white protease and green inhibitor. (A) Proteins with significantly altered abundances between the three groups were identified by ANOVA with $p < 0.05$. Each column represents a distinct heart group, as indicated at the top. Each row represents a unique protein. Each row is scaled with a z-score and colored to indicate the protein abundance changes across each column. Blue represents low, and orange represents high relative protein abundance. Rows are grouped based on hierarchical analysis by one minus Pearson's clustering, with each protein abundance pattern indicated on the right. (B) Gene ontology enrichment is shown for unique protein abundance patterns as a bar graph. The number of proteins in each pathway are indicated in brackets. Pathways significantly enriched are identified based on $p < 0.05$. A detailed list of proteins and gene ontology analysis is provided in Supporting Information 2 and 3. Five biological replicates from each group were investigated.

included all proteins for reference, depicted as a heatmap (Figure S5).

Seven unique protein abundance patterns are indicated to the right of the heatmap by line diagrams (Figure 3A, groups I–VII). A bar graph displays the corresponding enriched gene ontology pathways (Figure 3B).[32] Proteins with decreased abundance following IR injury are of particular interest (groups I, II, and V). In group I, ARP-100 had no significant effect on restoring the protein abundance, suggesting that MMP-2 does not play a role in modulating the abundance of these proteins. In groups II and V, ARP-100 significantly attenuated the proteins to those seen in the AER group. Thus, MMP-2 could be involved in the loss of these proteins following IR. These proteins include cofilin-1, complex III assembly factor LYRM7, ATP synthase membrane lipid-binding protein, glutaryl-CoA dehydrogenase, and methionine-R-sulfoxide reductase B2. Each of these proteins plays a role in tissue remodeling, contractile function, or mitochondrial function/energy metabolism. A complete list of all proteins identified within each group is presented (Supporting Information 2).

We aimed to further characterize the abundance changes of proteins measured with DIA mass spectrometry. We reinjected the same samples ($n = 5$) using DDA LC–MS/MS. The overlap of quantified proteins and scaled data (z-score) for select proteins are shown (Figure S6). Then, we further characterized selected proteins using immunoblots compared with DIA LC–MS/MS data. We chose proteins previously implicated in IR injury with reliable and commercially available antibodies. Representative immunoblots ($n = 6$) are presented in Figure S7. The bar graphs depict protein quantification using immunoblots (white) compared with LC–MS/MS (blue). First, we selected a protein with consistent levels in all three groups by LC–MS/MS. The protein abundance of 60 kDa heat shock protein (CH60) was measured by immunoblotting and found to be similar in all three heart groups as well (Figure S7A). Second, we observed a decrease in the abundance of adenylate kinase 1 (KAD1) in IR ($P < 0.05$) measured by LC–MS/MS. No significant changes were observed by immunoblot analysis (Figure S7A, middle panel). Next, we observed a nonsignificant decrease in the abundance of LDHA in IR hearts measured by LC–MS/MS and a subsequent increase in IR + ARP-100 measured by immunoblotting ($p < 0.06$) (Figure S7B). We observed no changes in α-actinin 2 (ACTN2) measured by LC–MS/MS and immunoblotting (Figure S7C, top panel). Then, we observed a decrease in serpin H1 (SERPH) in IR + ARP-100 hearts measured by LC–MS/MS and immunoblotting ($P < 0.05$) (Figure S7C, middle panel). Finally, we observed increased levels of myosin light chain 4 (MYL4) in IR measured by immunoblotting ($p < 0.05$) but an increase in IR + ARP-100 hearts measured by LC–MS/MS ($p < 0.01$) (Figure S7D). Factors explaining these incongruities may include multiple protein isoforms, varying antibody stability and specificity, higher limits of detection, and the limited linear dynamic range of immunoblotting.[41]

N-Terminomics Following IR Injury

We then extracted ventricular proteins using 1% SDS, which is necessary for compatibility with subtiligase reagents. We labeled the newly formed N-termini of cleaved proteins using subtiligase-mediated N-terminomics. We enriched for labeled (cleaved) proteins on neutravidin beads and digested them into semitryptic peptides on the beads. We eluted and desalted the labeled peptides, followed by LC–MS/MS. We identified 132 to 149 cleavage sites in each heart group among >1500 peptides (Figure 1C) with $a > 60\%$ overlap between biological replicates (Figure S8A–C). We found 15 cleavage sites unique to the IR injury group and 18 unique to IR + ARP-100 (Figure 4A). For simplicity, we denote proteins cleaved following IR ± ARP-100 with the mathematical symbol for "intersection" (∩). Out of all of the identified peptides (labeled and unlabeled), 7–14% contained labeled N-termini representing an average of 1.3 cleavage sites on each identified protein substrate (Figure S8D). A complete list of all cleavage sites and the overlap between heart groups is presented in Supporting Information 6. Cleavage sites are identified based on Schechter and Berger nomenclature, where residues surrounding cleavage are denoted as P4–P3–P2–P1↓P1′–P2′–P3′–P4′ (Figure S9A).[42] We used IceLogos to display the specificity of observed cleavage events for each heart group (Figure S9B–G). Enriched amino acids appear above the x-axis, and de-

https://doi.org/10.1021/acs.jproteome.3c00754
J. Proteome Res. 2024, 23, 844–856

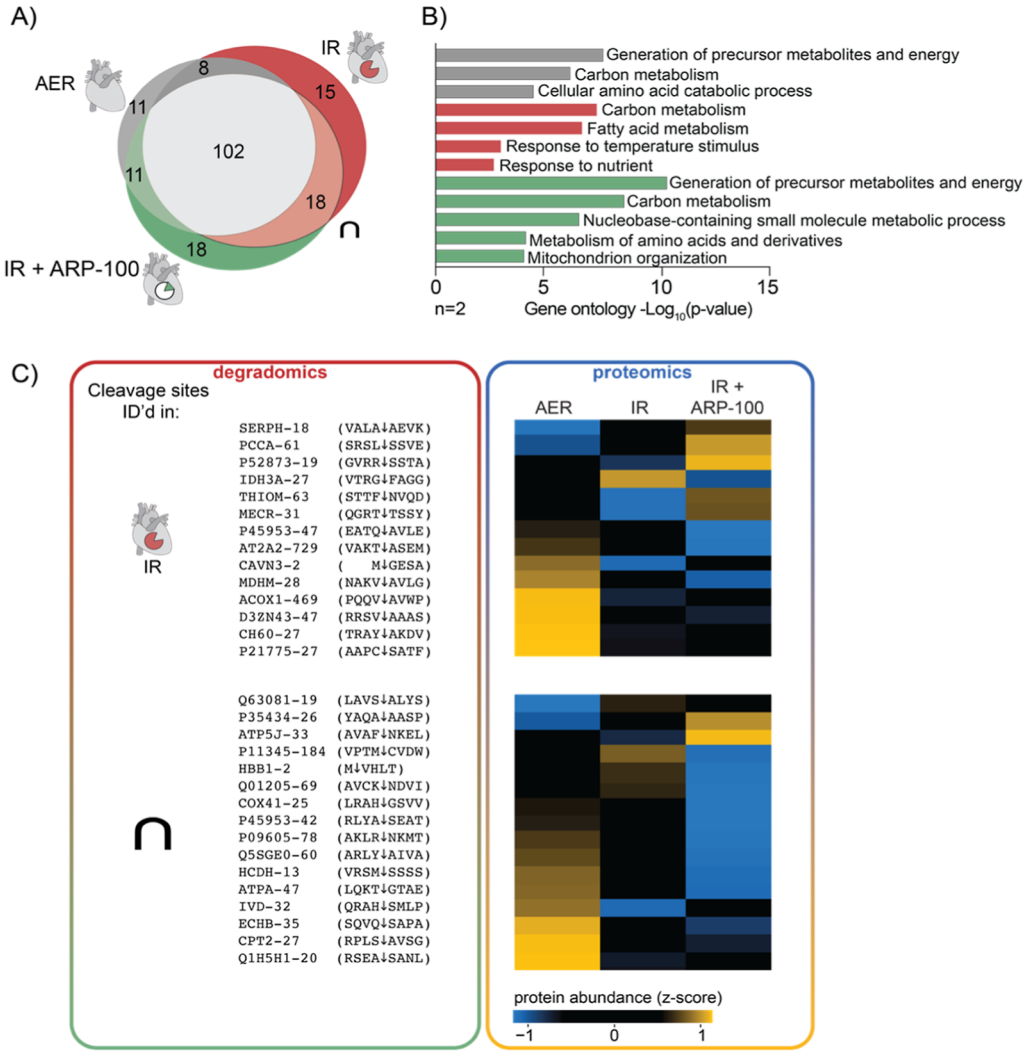

Figure 4. Results from the degradomics workflow showing proteolytic changes in ventricular extracts from the AER, IR, and IR + ARP-100 heart groups. N-terminomic labeling enables the identification of proteolytic sites following IR ± ARP-100. AER is represented by a gray heart, IR by a gray heart with a red protease, and IR + ARP-100 with a white protease and green inhibitor. (A) Number of unique cleavage sites identified in each group is depicted. 11, 15, and 18 cleavage sites were only identified in AER, IR, and IR + ARP-100, respectively. (B) Gene ontology protein enrichment is displayed for unique cleavage sites identified only in AER (gray), only IR (red), and only IR + ARP-100 (green) with $p < 0.05$. (C) Proteins that were cleaved in IR and IR + ARP-100 heart groups are identified by their UniProt ID with the cleavage site (P4−P4′) (left). The degradome and proteome changes are compared, whereby proteome changes (right panel) are depicted as a heatmap. Each column represents a heart group, and each row represents a unique protein. For simplicity, we denote proteins cleaved in IR and IR + ARP-100 hearts with the mathematical symbol for "intersection" (∩). Each row is colored to indicate the protein abundance changes across each column. Blue represents low, and orange represents high relative protein abundance. A detailed list of the cleavage sites, gene ontology, and heatmap is provided in Supporting Information 6 and 7. Two biological replicates from each group were used.

enriched ones appear below. Unsurprisingly, the sequence specificity of each group (all peptides) was found to be identical (Figure S9B−D). By looking at only the unique cleavage sites, we observed some small differences. For example, we observed two Ala residues at P1 and P1′ for the AER hearts (Figure S9E), compared to Gly/Arg/Tyr at P1 for the IR hearts. We noted the preference for small residues (P1′ = S/A) (Figure S9G) in all three groups, but this is likely due to subtiligase specificity.[30] Overall, the cleavage site specificity between all three groups is similar, and we cannot identify one specific protease responsible for any of the cleavages.

We performed gene ontology[32] on cleavage sites identified unique to AER (gray), IR (red), and IR + ARP-100 (green). We observed that proteins cleaved in IR injury are involved in metabolism and in response to temperature and nutrition stimuli. Among these is malate dehydrogenase (MDH), which is a known MMP-2 substrate in vitro.[43,44] In IR + ARP-100 hearts, cleaved proteins are involved in metabolism and mitochondrial organization (Figure 4B).

Comparative Analysis of Proteomics and Degradomics in Rat Hearts Following IR Injury ± ARP-100

After analyzing the degradome and proteome, we found 14 cleaved proteins following IR injury, corresponding to 15 cleavage sites since enoyl-[acyl-carrier-protein] reductase was cleaved at two sites. All of which were also quantified in the proteomics workflow. One of the proteins, CH60, was cleaved following residue 27 (TRAY↓AKDV). However, we observed a nonsignificant decrease in abundance in the proteomics approach. Another protein, SERPH, was cleaved following residue 18 (VALA↓AEVK), and we observed a nonsignificant

https://doi.org/10.1021/acs.jproteome.3c00754
J. Proteome Res. 2024, 23, 844−856

increase in abundance in the proteomics approach (Figure 4C, top panel). Of the 18 proteins cleaved following IR ± ARP-100 (denoted by "∩"), we quantified 17 in the proteomics approach. We did not quantify the protein level of mediator of RNA polymerase II transcription subunit 2, which may be due to differences in protein extraction methods (Figure 4C, lower panel). These data highlight the requirement for both proteomics and degradomics approaches as degradome changes are not always reflected in the proteome. This is potentially due to a small proportion of the protein being degraded in many cases.

DISCUSSION

The pathophysiology of oxidative stress in cardiac IR injuries is well established. For example, reperfusion exacerbates the damage following ischemia by generating and releasing reactive oxygen/nitrogen species (RONS).[45−49] Further intracellular damage can occur by RONS-induced activation of proteases, such as MMP-2.[50,51] We observed significant changes in the abundance and cleavage of several proteins involved in RONS handling and generation (Figure 5). For example, the abundance of methionine-R-sulfoxide reductase B2, which reduces oxidative stress, decreased following IR injury (fold change = 1.4, p-value = 0.003). Its levels increased in the IR + ARP-100 hearts. This observation is consistent with previous reports, indicating that its activity decreased during ischemia and early reperfusion.[52]

L

Oxidative stress further modulates fatty acid metabolism in cardiomyocytes. For example, the conversion of fatty acyl-CoA into acetyl-CoA is coupled with hydrogen peroxide production in peroxisomes.[53−55] Several peroxisomal proteins decreased in abundance or were found to be cleaved following IR injury, such as peroxisomal acyl-coenzyme A oxidase 1 and THIKA. Interestingly, inhibition of THIKA is suggested to be cardioprotective.[56] Although this is the first report of cleavage site identification of these proteins following IR injury, previous studies report modulation of proteins involved in fatty acid metabolism.[57,58]

Metabolic dysfunction is a well-documented consequence of cardiac IR injury (see[59−62]). The lack of oxygen and altered calcium homeostasis impact pyruvate and fatty acid oxidation, and oxidative phosphorylation.[63] Here, we found numerous proteins involved in the metabolism of pyruvate that were altered in abundance or identified by N-terminomics (Figure 5), such as pyruvate carboxylase, MDH, and LDH. The abundance of LDH in IR injury is however controversial, where its cleavage and secretion have been reported.[19] LDH converts pyruvate to lactate under anaerobic conditions. We found that LDH levels were not significantly altered following IR injury. On the contrary, in a report utilizing 2D-gel electrophoresis, its levels increased after IR.[7] This study, however, used 15 min of no-flow or 60 min of low-flow ischemia in rabbit hearts. This discrepancy might also be explained by the different methodologies used, for both protein extraction and data acquisition. It is worth mentioning that we also observed a decrease in LDH levels in IR injury using data-dependent acquisition (data not shown). For an explanation on differences between data-dependent and DIA in mass spectrometry, see[64,65] for reviews.

Under aerobic conditions, pyruvate enters the tricarboxylic acid cycle as acetyl-CoA or oxaloacetate.[66] Alternatively, fatty acyl CoA can be converted to acetyl-CoA. We identified the

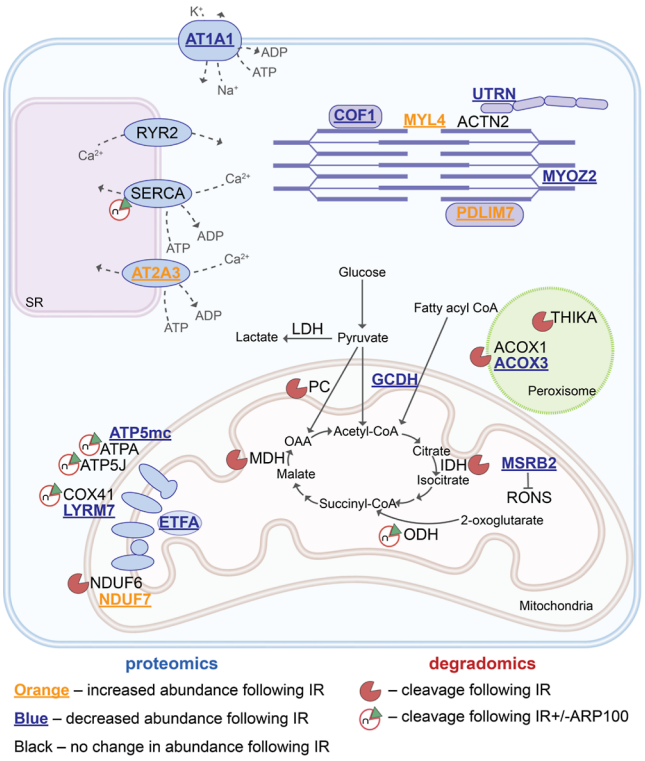

Figure 5. Proteins involved in metabolism and cardiac muscle contraction show differential protein abundances and cleavage patterns following myocardial IR injury. Some proteins involved in the tricarboxylic acid cycle, electron transport chain, and cardiac muscle contraction, among others, are cleaved following myocardial IR injury. Proteins are labeled by their UniProt ID and defined below. Proteins with decreasing or increasing abundances following myocardial IR injury are denoted by blue or orange letters, respectively. A red protease "Pac-Man" represents cleavage following IR, and a white protease with a green triangle represents cleavage following IR and IR + ARP-100. Proteins displayed are those involved in the mentioned pathways with significant changes in abundance, based on Student's t test used in volcano plot analysis, or that are cleaved, based on gene ontology analysis with $p < 0.05$. Proteins are denoted as follows: 3-ketoacyl-CoA thiolase A (THIKA), actinin alpha 2 (ACTN2), adenylate kinase isoenzyme 1 (KAD1), ATP synthase membrane lipid-binding protein (ATP5mc), ATP synthase subunit alpha (ATPA), ATP synthase-coupling factor 6 (ATP5J), cofilin-1 (COF1), complex III assembly factor LYRM7 (LYRM7), cytochrome c oxidase subunit 4 isoform 1 (COX41), D-dopachrome decarboxylase (ODH), electron transfer flavoprotein subunit alpha (ETFA), glutaryl-CoA dehydrogenase (GCDH), isocitrate dehydrogenase (IDH), L-lactate dehydrogenase (LDH), malate dehydrogenase (MDH), methionine-R-sulfoxide reductase B2 (MSRB2), myosin light chain 4 (MYL4), myozenin-2 (MYOZ2), NADH dehydrogenase complex I assembly factor 6 (NDUF6), NADH dehydrogenase complex I assembly factor 7 (NDUF7), PDZ and LIM domain protein 7 (PDLIM7), peroxisomal acyl-coenzyme A oxidase 1 (ACOX1), pyruvate carboxylase (PC), ryanodine receptor 2 (RyR2), sarcoplasmic/endoplasmic reticulum calcium ATPase 3 (AT2A3), sarcoplasmic/endoplasmic reticulum calcium ATPase 2 (SERCA) sodium/potassium-transporting ATPase subunit alpha-1 (AT1A1), and utrophin (UTRN).

cleavage of both IDH and MDH (Figure 5). The role of IDH in IR injury and hypoxia-reoxygenation has been well documented, although proteolysis has not been previously reported.[67−69] MDH, on the other hand, is a known MMP-2 substrate, as determined in vitro by identifying its cleavage site

https://doi.org/10.1021/acs.jproteome.3c00754
J. Proteome Res. 2024, 23, 844−856

by LC−MS/MS analysis of a protein library.[43,44,70] Following the citric acid cycle, intermediates proceed to the electron transport chain to produce ATP via oxidative phosphorylation. The involvement of these pathways in myocardial IR injury has been previously reported,[7,10] including the release of RONS through complex I disrupting ATP generation.[48,49,71] We observed a decrease in electron-transfer flavoprotein subunit alpha abundance and an increase of NADH dehydrogenase complex I assembly factor 7. We also observed cleavage of complex I assembly factor 6. Inhibition of RONS release through complex I has been shown to prevent IR injury.[72,73]

Metabolic alterations following myocardial IR injury are ultimately linked to cardiac contraction, which is maintained by excitation-contraction coupling.[74] When intracellular calcium levels increase during IR,[75] sarcomeric proteins are affected, leading to contractile dysfunction.[76,77] Consistent with this, we observed a decrease in the abundance of several myocardial proteins, including sodium- and potassium-transporting ATPase 3, cofilin-1, cofilin-2, and utrophin, in IR hearts. Interestingly, we found an increase in cofilin-1 in IR hearts treated with ARP-100. Cofilins contribute to actin remodeling and depolymerization.[78,79] Cofilin-1 is expressed ubiquitously, while cofilin-2 is mostly expressed in cardiomyocytes in the heart.[80] Interestingly, the overexpression of cofilin-2 has been shown to promote the accumulation of stress fibers and diminish cardiac contractility in dilated cardiomyopathy. Aggregates enriched in cofilin-2 were found in hearts of patients with dilated cardiomyopathy.[81] It is possible that ischemic events trigger myocardial aggregate deposition, and defining cofilins' precise role in this process would be worth exploring.

In summary, we employed state-of-the-art mass spectrometry methods that until now have not been used to assess the proteome and degradome following cardiac IR injury. Using DIA proteomics and N-terminomics methods, we investigated the proteome and degradome changes following IR injury in isolated working rat hearts and the effects of MMP-2 inhibition. Here, we found significant alterations in the abundance of 447 proteins and a total of 183 unique cleavage sites between all of the heart groups. Proteins altered are involved in four major pathways: RONS handling and generation, fatty acid metabolism, mitochondrial function and metabolism, and cardiomyocyte contraction. Alterations in these pathways may result in the development of mitochondrial and cardiac contractile dysfunctions.

The proteomics approach presented in this study is a powerful method to assess thousands of proteins simultaneously. We also provide here a comprehensive comparison between the proteome changes reported in this study and those previously identified in hypoxia-reoxygenation or IR injury (Table S1, of Supporting Information). Supporting our proteomics data, we present immunoblots of select proteins identified with reliable and commercially available antibodies. We further confirmed protein changes using DDA. We noted some discrepancies between mass spectrometry and immunoblot quantification. Factors explaining this include varying antibody stability and specificity, higher limits of detection, and limited linear dynamic ranges of immunoblotting.[41] The data shown also highlight the inconsistencies arising from the use of various loading controls. The choice of loading control may have a significant impact on quantification by immunoblotting, which has been discussed in detail elsewhere.[82]

The degradomics approach presented in this study is an effective method to assess proteolytic cleavage sites in biological systems. We also provide here a comprehensive comparison between the cleavage sites identified in IR injury in the N-terminomics workflow and previously identified MMP-2 substrates (Table S2, of Supporting Information), suggesting that MMP-2 cleaves proteins, including SERPH, CH60, and THIO, during IR injury. We expected to see a decrease in the total number of cleavage sites identified with the ARP-100 treatment, which was not the case. This observation may be due to incomplete MMP-2 inhibition or imperfect lysis conditions where we used 1% SDS. Furthermore, cleavage sites reported in AER heart extracts are likely from protein turnover/degradation, which may be enhanced by the background oxidative stress of isolated heart perfusion.[83]

We inhibited MMP-2 with ARP-100 during cardiac IR injury and quantified protein levels using LC−MS/MS. Interestingly, a subset of proteins increased or decreased in abundance only in the IR + ARP-100 group. These proteins could represent the unexpected side effects of ARP-100, but additional controls of aerobic hearts with ARP-100 administration could be used in future studies to address this possibility. Unexpectedly, in the N-terminomics workflow, we identified more cleavage sites in IR + ARP-100 hearts than that in IR alone. Numerous factors may contribute to this observation, including the stochasticity of the N-terminomics experiments (Figure S8), the intrinsic bias of subtiligase labeling,[30] or incomplete MMP-2 inhibition.

The number of identified cleavage sites is low compared to reports in cell extracts from cell lines.[84,85] This is the first use of subtiligase N-terminomics in heart tissue, which is highly complex, containing numerous cell types and a connective matrix. Further optimization may be necessary to improve the coverage of proteolytic substrates. Although subtiligase-mediated N-terminomics is robust with low false discovery rates, one key limitation is the inherent substrate specificity of subtiligase on the prime side of cleavage sites.[29] This is partly attenuated by the use of mutant subtiligase strains which broaden the subtiligase labeling specificity.[30] Further optimization of the subtiligase-based system or the use of other N-terminomics methods may improve the cleavage site identification in cardiac systems and should be a focus point for future research.

The combination of proteomics and degradomics in this study provides a comprehensive understanding of the underlying biochemical alterations resulting from IR injury. Proteomics provides a baseline for altered proteins; however, it does not provide information as to why these proteins are changing in abundance. Degradomics provides specific insights into functional proteomics. Proteolytic processing is a form of irreversible post-translational modification, which may only effect a small proportion of a protein, and thus is not always reflected in the proteome. By presenting both data sets, we further uncovered biochemical alterations in key functional pathways: RONS handling and generation, fatty acid metabolism, mitochondrial function and metabolism, and cardiomyocyte contraction. Alterations of proteins within these pathways during IR would contribute to the resulting cardiac contractile dysfunction. For example, alterations of proteins in the electron transport chain may affect ATP generation and, subsequently, the activity of proteins dependent on ATP (for example, SERCA). Furthermore, the observed cleavage of SERCA2a or increased sodium- or potassium-transporting ATPase abundance may affect calcium handling

https://doi.org/10.1021/acs.jproteome.3c00754
J. Proteome Res. 2024, 23, 844−856

and contraction. Further impacting contraction are the proteins interacting with the contractile unit: cofilin-1, utrophin, and PDZ and LIM domain protein 7, all of which were altered in abundance during IR injury.

This study focuses on the role of MMP-2 in myocardial IR injury by pharmacological inhibition with ARP-100. However, other intracellular proteases, such as calpains, cathepsins, caspases, and other MMPs, may be responsible for the proteome and degradome changes. For example, during ischemia, an increase in intracellular pH ultimately leads to the downstream activation of the Na^+/Ca^{2+} exchanger protein, which increases intracellular calcium, resulting in calpain activation.[3,86] Similar events have been reported in other cardiomyopathies, such as arrhythmogenic cardiomyopathy.[87] Here, we report the abundance of 15 proteases, three of which were significantly changed: mitochondrial intermediate peptidase, endoplasmic reticulum metallopeptidase 1, and cystatin C following IR injury. However, as many proteases are expressed as zymogens, other proteases could still be activated without changes in protein abundance. One avenue of future research would be to investigate the proteome and degradome changes resulting from IR with other protease inhibitors, such as those targeting calpain family members.

CONCLUSIONS

These findings uncover information about the intracellular pathology of myocardial IR injury using the most recent mass spectrometry approaches. We have uncovered the protein abundance levels of thousands of proteins and identified new proteolytic targets, including those of MMP-2. Understanding the intracellular mechanisms of IR injury is crucial for translational medicine as gaps in knowledge prevent preclinical data from being translated into clinical practice. This research can serve as a baseline for future studies on implicated proteases, inhibitor design, and other therapeutic strategies.

ASSOCIATED CONTENT

Supporting Information

The Supporting Information is available free of charge at https://pubs.acs.org/doi/10.1021/acs.jproteome.3c00754.

Additional experimental details, materials, and methods; physiological parameters of heart contractile performance immediately prior to the onset of ischemia and at the end of reperfusion; DIA mass spectrometry allowed for the quantification of a wide range of subcellular proteins with high reproducibility; relative proteome changes in ventricular lysates following ischemia-reperfusion with or without the MMP-2 selective inhibitor, ARP-100; distinct enrichment of gene ontology pathways in hearts following ischemia-reperfusion with or without the MMP-2 inhibitor, ARP-100; all proteins quantified in ventricular extracts prepared from hearts following IR with or without the MMP-2 selective inhibitor, ARP-100; DDA used to confirm protein abundance measured by DIA LC−MS/MS; immunoblotting indicating distinct protein abundance patterns of selected proteins; proteolytic changes in the heart following ischemia-reperfusion with or without the MMP-2 selective inhibitor, ARP-100; distinct sequence motifs in hearts with ischemia-reperfusion with and without the MMP-2 inhibitor, ARP-100; full immunoblots used to indicate distinct protein abundance patterns of selected proteins; comparison of proteome levels to previously published protein levels following IR injury, quantified using mass spectrometry; and comparison of the identified proteome and degradome changes in all three heart groups (MEROPS database used to cross-reference identified MMP-2 cleavage sites) (PDF)

Complete spectra search output and unprocessed Spectronaut output (XLSX)

Quantification and scaling of whole lysates used in heatmaps (XLSX)

Gene ontology corresponding to heatmaps (XLSX)

Quantification and scaling of whole lysates used in volcano plots (XLSX)

Gene ontology corresponding to volcano plots (XLSX)

Identification of protein substrates (XLSX)

Gene ontology corresponding to identified protein substrates (XLSX)

AUTHOR INFORMATION

Corresponding Authors

Richard Schulz − *Department of Pharmacology and Department of Pediatrics, University of Alberta, Edmonton T6G 2S2, Canada*; Email: richard.schulz@ualberta.ca

Olivier Julien − *Department of Biochemistry, University of Alberta, Edmonton T6G 2H7, Canada*; orcid.org/0000-0001-7068-7299; Email: ojulien@ualberta.ca

Authors

Bridgette Hartley − *Department of Biochemistry, University of Alberta, Edmonton T6G 2H7, Canada*; orcid.org/0000-0002-9883-952X

Wesam Bassiouni − *Department of Pharmacology, University of Alberta, Edmonton T6G 2S2, Canada*

Andrej Roczkowsky − *Department of Pharmacology, University of Alberta, Edmonton T6G 2S2, Canada*

Richard Fahlman − *Department of Biochemistry, University of Alberta, Edmonton T6G 2H7, Canada*

Complete contact information is available at: https://pubs.acs.org/10.1021/acs.jproteome.3c00754

Notes

The authors declare no competing financial interest.

ACKNOWLEDGMENTS

We thank Jack Moore and the Alberta Proteomics and Mass Spectrometry Facility for technical support. We received funding from the Canadian Institutes of Health Research (FDN-143299 to R.S.), the Canadian Foundation for Innovation (37833 and 39051 to O.J.) and Natural Sciences, Engineering Research Council of Canada (DGECR-2018-00142 discovery grant to O.J.), and the Alberta Graduate Excellence Scholarship (B.H.).

ABBREVIATIONS

IR, ischemia-reperfusion; LC-MS/MS, liquid chromatography-tandem mass spectrometry; DIA, data-independent acquisition; MMP, matrix metalloproteinase; RONS, reactive oxygen/nitrogen species; Abu, aminobutyric acid

REFERENCES

(1) Tsao, C. W.; Aday, A. W.; Almarzooq, Z. I.; Alonso, A.; Beaton, A. Z.; Bittencourt, M. S.; Boehme, A. K.; Buxton, A. E.; Carson, A. P.; Commodore-Mensah, Y.; Elkind, M. S. V.; Evenson, K. R.; Eze-Nliam, C.; Ferguson, J. F.; Generoso, G.; Ho, J. E.; Kalani, R.; Khan, S. S.; Kissela, B. M.; Knutson, K. L.; Levine, D. A.; Lewis, T. T.; Liu, J.; Loop, M. S.; Ma, J.; Mussolino, M. E.; Navaneethan, S. D.; Perak, A. M.; Poudel, R.; Rezk-Hanna, M.; Roth, G. A.; Schroeder, E. B.; Shah, S. H.; Thacker, E. L.; VanWagner, L. B.; Virani, S. S.; Voecks, J. H.; Wang, N. Y.; Yaffe, K.; Martin, S. S. Heart disease and stroke statistics-2022 update: A report from the American heart association. *Circulation* **2022**, *145*, No. e153-e639.

(2) Libby, P. Current concepts of the pathogenesis of the acute coronary syndromes. *Circulation* **2001**, *104*, 365−372.

(3) Hausenloy, D. J.; Yellon, D. M. Myocardial ischemia-reperfusion injury: a neglected therapeutic target. *J. Clin. Invest.* **2013**, *123*, 92−100.

(4) Thygesen, K.; Alpert, J. S.; Jaffe, A. S.; Chaitman, B. R.; Bax, J. J.; Morrow, D. A.; White, H. D. Fourth Universal Definition of Myocardial Infarction (2018). *J. Am. Coll. Cardiol.* **2018**, *72*, 2231−2264.

(5) McCarthy, C. P.; Raber, I.; Chapman, A. R.; Sandoval, Y.; Apple, F. S.; Mills, N. L.; Januzzi, J. L. Myocardial injury in the era of high-sensitivity cardiac troponin assays: A practical approach for clinicians. *JAMA Cardiol.* **2019**, *4*, 1034−1042.

(6) Bolli, R.; Marbán, E. Molecular and cellular mechanisms of myocardial stunning. *Physiol. Rev.* **1999**, *79*, 609−634.

(7) White, M. Y.; Cordwell, S. J.; McCarron, H. C.; Prasan, A. M.; Craft, G.; Hambly, B. D.; Jeremy, R. W. Proteomics of ischemia/reperfusion injury in rabbit myocardium reveals alterations to proteins of essential functional systems. *Proteomics* **2005**, *5*, 1395−1410.

(8) Wang, X.; Shen, X.; Weil, B. R.; Young, R. F.; Canty, J. M.; Qu, J. Quantitative proteomic and phosphoproteomic profiling of ischemic myocardial stunning in swine. *Am. J. Physiol.: Heart Circ. Physiol.* **2020**, *318*, 1256−1271.

(9) Sawicki, G.; Leon, H.; Sawicka, J.; Sariahmetoglu, M.; Schulze, C. J.; Scott, P. G.; Szczesna-Cordary, D.; Schulz, R. Degradation of myosin light chain in isolated rat hearts subjected to ischemia-reperfusion injury: a new intracellular target for matrix metalloproteinase-2. *Circulation* **2005**, *112*, 544−552.

(10) Binek, A.; Fernández-Jiménez, R.; Jorge, I.; Camafeita, E.; López, J. A.; Bagwan, N.; Galán-Arriola, C.; Pun, A.; Agüero, J.; Fuster, V.; Ibanez, B.; Vázquez, J. Proteomic footprint of myocardial ischemia/reperfusion injury: Longitudinal study of the at-risk and remote regions in the pig model. *Sci. Rep.* **2017**, *7*, 12343.

(11) Doerr, A. DIA mass spectrometry. *Nat. Methods* **2015**, *12*, 35.

(12) Bruderer, R.; Bernhardt, O. M.; Gandhi, T.; Miladinović, S. M.; Cheng, L. Y.; Messner, S.; Ehrenberger, T.; Zanotelli, V.; Butscheid, Y.; Escher, C.; Vitek, O.; Rinner, O.; Reiter, L. Extending the limits of quantitative proteome profiling with data-independent acquisition and application to acetaminophen-treated three-dimensional liver microtissues. *Mol. Cell. Proteomics* **2015**, *14*, 1400−1410.

(13) Muntel, J.; Gandhi, T.; Verbeke, L.; Bernhardt, O. M.; Treiber, T.; Bruderer, R.; Reiter, L. Surpassing 10 000 identified and quantified proteins in a single run by optimizing current LC-MS instrumentation and data analysis strategy. *Mol. Omics* **2019**, *15*, 348−360.

(14) Poulos, R. C.; Hains, P. G.; Shah, R.; Lucas, N.; Xavier, D.; Manda, S. S.; Anees, A.; Koh, J. M. S.; Mahboob, S.; Wittman, M.; Williams, S. G.; Sykes, E. K.; Hecker, M.; Dausmann, M.; Wouters, M. A.; Ashman, K.; Yang, J.; Wild, P. J.; deFazio, A.; Balleine, R. L.; Tully, B.; Aebersold, R.; Speed, T. P.; Liu, Y.; Reddel, R. R.; Robinson, P. J.; Zhong, Q. Strategies to enable large-scale proteomics for reproducible research. *Nat. Commun.* **2020**, *11*, 3793.

(15) Wang, W.; Schulze, C. J.; Suarez-Pinzon, W. L.; Dyck, J. R. B.; Sawicki, G.; Schulz, R. Intracellular action of matrix metalloproteinase-2 accounts for acute myocardial ischemia and reperfusion injury. *Circulation* **2002**, *106*, 1543−1549.

(16) Katrukha, I. A.; Kogan, A. E.; Vylegzhanina, A. V.; Kharitonov, A. V.; Tamm, N. N.; Filatov, V. L.; Bereznikova, A. V.; Koshkina, E. V.; Katrukha, A. G. Full-size cardiac troponin I and its proteolytic fragments in blood of patients with acute myocardial infarction: antibody selection for assay development. *Clin. Chem.* **2018**, *64*, 1104−1112.

(17) Mahmud, Z.; Zahran, S.; Liu, P. B.; Reiz, B.; Chan, B. Y. H.; Roczkowsky, A.; McCartney, C. S. E.; Davies, P. L.; Li, L.; Schulz, R.; Hwang, P. M. Structure and proteolytic susceptibility of the inhibitory C-terminal tail of cardiac troponin I. *Biochim. Biophys. Acta, Gen. Subj.* **2019**, *1863*, 661−671.

(18) Gao, W. D.; Atar, D.; Liu, Y.; Perez, N. G.; Murphy, A. M.; Marban, E. Role of troponin I proteolysis in the pathogenesis of stunned myocardium. *Circ. Res.* **1997**, *80*, 393−399.

(19) Peng, K.; Liu, H.; Yan, B.; Meng, X. W.; Song, S. Y.; Ji, F. H.; Xia, Z. Inhibition of cathepsin S attenuates myocardial ischemia/reperfusion injury by suppressing inflammation and apoptosis. *J. Cell. Physiol.* **2021**, *236*, 1309−1320.

(20) Barta, J.; Tóth, A.; Edes, I.; Vaszily, M.; Papp, J. G.; Varró, A.; Papp, Z. Calpain-1-sensitive myofibrillar proteins of the human myocardium. *Mol. Cell. Biochem.* **2005**, *278*, 1−8.

(21) Communal, C.; Sumandea, M.; de Tombe, P.; Narula, J.; Solaro, R. J.; Hajjar, R. J. Functional consequences of caspase activation in cardiac myocytes. *Proc. Natl. Acad. Sci. U.S.A.* **2002**, *99*, 6252−6256.

(22) Ali, M. A.; Cho, W. J.; Hudson, B.; Kassiri, Z.; Granzier, H.; Schulz, R. Titin is a target of matrix metalloproteinase-2: implications in myocardial ischemia/reperfusion injury. *Circulation* **2010**, *122*, 2039−2047.

(23) Roczkowsky, A.; Chan, B. Y. H.; Lee, T. Y. T.; Mahmud, Z.; Hartley, B.; Julien, O.; Armanious, G.; Young, H. S.; Schulz, R. Myocardial MMP-2 contributes to SERCA2a proteolysis during cardiac ischaemia−reperfusion injury. *Cardiovasc. Res.* **2020**, *116*, 1021−1031.

(24) Singh, R. B.; Chohan, P. K.; Dhalla, N. S.; Netticadan, T. The sarcoplasmic reticulum proteins are targets for calpain action in the ischemic-reperfused heart. *J. Mol. Cell. Cardiol.* **2004**, *37*, 101−110.

(25) Sung, M. M.; Schulz, C. G.; Wang, W.; Sawicki, G.; Bautista-López, N. L.; Schulz, R. Matrix metalloproteinase-2 degrades the cytoskeletal protein α-actinin in peroxynitrite mediated myocardial injury. *J. Mol. Cell. Cardiol.* **2007**, *43*, 429−436.

(26) Matsumura, Y.; Saeki, E.; Inoue, M.; Hori, M.; Kamada, T.; Kusuoka, H. Inhomogeneous disappearance of myofilament-related cytoskeletal proteins in stunned myocardium of guinea pig. *Circ. Res.* **1996**, *79*, 447−454.

(27) Hartley, B.; Bassiouni, W.; Schulz, R.; Julien, O. The roles of intracellular proteolysis in cardiac ischemia-reperfusion injury. *Basic Res. Cardiol.* **2023**, *118*, 38.

(28) Hughes, B. G.; Schulz, R. Targeting MMP-2 to treat ischemic heart injury. *Basic Res. Cardiol.* **2014**, *109*, 424.

(29) Abrahmsen, L.; Tom, J.; Burnier, J.; Butcher, K. A.; Kossiakoff, A.; Wells, J. A. Engineering subtilisin and its substrates for efficient ligation of peptide bonds in aqueous solution. *Biochemistry* **1991**, *30*, 4151−4159.

(30) Weeks, A. M.; Wells, J. A. Engineering peptide ligase specificity by proteomic identification of ligation sites. *Nat. Chem. Biol.* **2018**, *14*, 50−57.

(31) Mahrus, S.; Trinidad, J. C.; Barkan, D. T.; Sali, A.; Burlingame, A. L.; Wells, J. A. Global sequencing of proteolytic cleavage sites in apoptosis by specific labeling of protein N termini. *Cell* **2008**, *134*, 866−876.

(32) Zhou, Y.; Zhou, B.; Pache, L.; Chang, M.; Khodabakhshi, A. H.; Tanaseichuk, O.; Benner, C.; Chanda, S. K. Metascape provides a biologist-oriented resource for the analysis of systems-level datasets. *Nat. Commun.* **2019**, *10*, 1523.

(33) Barter, R.; Yu, B.; Barter, M. R. Package 'superheat' A graphical tool for exploring complex datasets using heatmaps. *arXiv* **2017**, arXiv:1512.01524v2 Version 0.1. 0.

(34) Rossello, A.; Nuti, E.; Orlandini, E.; Carelli, P.; Rapposelli, S.; Macchia, M.; Minutolo, F.; Carbonaro, L.; Albini, A.; Benelli, R.; et al. New N-arylsulfonyl-N-alkoxyaminoacetohydroxamic acids as selective

https://doi.org/10.1021/acs.jproteome.3c00754
J. Proteome Res. 2024, 23, 844−856

inhibitors of gelatinase A (MMP-2). *Bioorg. Med. Chem.* **2004**, *12*, 2441−2450.
(35) Tuccinardi, T.; Martinelli, A.; Nuti, E.; Carelli, P.; Balzano, F.; Uccello-Barretta, G.; Murphy, G.; Rossello, A. Amber force field implementation, molecular modelling study, synthesis and MMP-1/MMP-2 inhibition profile of (R)- and (S)-N-hydroxy-2-(N-isopropoxybiphenyl-4-ylsulfonamido)-3-methylbutanamides. *Bioorg. Med. Chem.* **2006**, *14*, 4260−4276.
(36) Ali, M. A. M.; Garcia-Vilas, J. A.; Cromwell, C. R.; Hubbard, B. P.; Hendzel, M. J.; Schulz, R. Matrix metalloproteinase-2 mediates ribosomal RNA transcription by cleaving nucleolar histones. *FEBS J.* **2021**, *288*, 6736−6751.
(37) Belliard, A.; Sottejeau, Y.; Duan, Q.; Karabin, J. L.; Pierre, S. V. Modulation of cardiac Na+,K+-ATPase cell surface abundance by simulated ischemia-reperfusion and ouabain preconditioning. *Am. J. Physiol.: Heart Circ. Physiol.* **2013**, *304*, H94−H103.
(38) Okawa, H.; Horimoto, H.; Mieno, S.; Nomura, Y.; Yoshida, M.; Shinjiro, S. Preischemic infusion of alpha-human atrial natriuretic peptide elicits myoprotective effects against ischemia reperfusion in isolated rat hearts. *Mol. Cell. Biochem.* **2003**, *248*, 171−177.
(39) Crambert, G.; Fuzesi, M.; Garty, H.; Karlish, S.; Geering, K. Phospholemman (FXYD1) associates with Na,K-ATPase and regulates its transport properties. *Proc. Natl. Acad. Sci. U.S.A.* **2002**, *99*, 11476−11481.
(40) Wang, J.; Song, J.; Gao, E.; Zhang, X. Q.; Gu, T.; Yu, D.; Koch, W. J.; Feldman, A. M.; Cheung, J. Y. Induced overexpression of phospholemman S68E mutant improves cardiac contractility and mortality after ischemia-reperfusion. *Am. J. Physiol.: Heart Circ. Physiol.* **2014**, *306*, H1066−H1077.
(41) Aebersold, R.; Burlingame, A. L.; Bradshaw, R. A. Western blots versus selected reaction monitoring assays: time to turn the tables. *Mol. Cell. Proteomics* **2013**, *12*, 2381−2382.
(42) Schechter, I.; Berger, A. On the size of the active site in proteases. I. Papain. *Biochem. Biophys. Res. Commun.* **1967**, *27*, 157−162.
(43) Schilling, O.; Overall, C. M. Proteome-derived, database-searchable peptide libraries for identifying protease cleavage sites. *Nat. Biotechnol.* **2008**, *26*, 685−694.
(44) Kleifeld, O.; Doucet, A.; auf dem Keller, U.; Prudova, A.; Schilling, O.; Kainthan, R. K.; Starr, A. E.; Foster, L. J.; Kizhakkedathu, J. N.; Overall, C. M. Isotopic labeling of terminal amines in complex samples identifies protein N-termini and protease cleavage products. *Nat. Biotechnol.* **2010**, *28*, 281−288.
(45) Yasmin, W.; Strynadka, K. D.; Schulz, R. Generation of peroxynitrite contributes to ischemia-reperfusion injury in isolated rat hearts. *Cardiovasc. Res.* **1997**, *33*, 422−432.
(46) Davies, K. J. The oxygen paradox, oxidative stress, and ageing. *Arch. Biochem. Biophys.* **2016**, *595*, 28−32.
(47) Zorov, D. B.; Juhaszova, M.; Sollott, S. J. Mitochondrial reactive oxygen species (ROS) and ROS-induced ROS release. *Physiol. Rev.* **2014**, *94*, 909−950.
(48) Abramov, A. Y.; Scorziello, A.; Duchen, M. R. Three distinct mechanisms generate oxygen free radicals in neurons and contribute to cell death during anoxia and reoxygenation. *J. Neurosci.* **2007**, *27*, 1129−1138.
(49) Murphy, M. P. How mitochondria produce reactive oxygen species. *Biochem. J.* **2009**, *417*, 1−13.
(50) Okamoto, T.; Akaike, T.; Sawa, T.; Miyamoto, Y.; van der Vliet, A.; Maeda, H. Activation of matrix metalloproteinases by peroxynitrite-induced protein S-glutathiolation via disulfide S-oxide formation. *J. Biol. Chem.* **2001**, *276*, 29596−29602.
(51) Viappiani, S.; Nicolescu, A. C.; Holt, A.; Sawicki, G.; Crawford, B. D.; León, H.; van Mulligen, T.; Schulz, R. Activation and modulation of 72 kDa matrix metalloproteinase-2 by peroxynitrite and glutathione. *Biochem. Pharmacol.* **2009**, *77*, 826−834.
(52) Picot, C. R.; Perichon, M.; Lundberg, K. C.; Friguet, B.; Szweda, L. I.; Petropoulos, I. Alterations in mitochondrial and cytosolic methionine sulfoxide reductase activity during cardiac ischemia and reperfusion. *Exp. Gerontol.* **2006**, *41*, 663−667.
(53) Chen, X. F.; Tian, M. X.; Sun, R. Q.; Zhang, M. L.; Zhou, L. S.; Jin, L.; Chen, L. L.; Zhou, W. J.; Duan, K. L.; Chen, Y. J.; Gao, C.; Cheng, Z. L.; Wang, F.; Zhang, J. Y.; Sun, Y. P.; Yu, H. X.; Zhao, Y. Z.; Yang, Y.; Liu, W. R.; Shi, Y. H.; Xiong, Y.; Guan, K. L.; Ye, D. SIRT5 inhibits peroxisomal ACOX1 to prevent oxidative damage and is downregulated in liver cancer. *EMBO Rep.* **2018**, *19*, No. e45124.
(54) Zeng, J.; Li, D. Expression and purification of his-tagged rat peroxisomal acyl-CoA oxidase I wild-type and E421 mutant proteins. *Protein Expression Purif.* **2004**, *38*, 153−160.
(55) Bienert, G. P.; Schjoerring, J. K.; Jahn, T. P. Membrane transport of hydrogen peroxide. *Biochim. Biophys. Acta* **2006**, *1758*, 994−1003.
(56) Kantor, P. F.; Lucien, A.; Kozak, R.; Lopaschuk, G. D. The antianginal drug trimetazidine shifts cardiac energy metabolism from fatty acid oxidation to glucose oxidation by inhibiting mitochondrial long-chain 3-ketoacyl coenzyme A thiolase. *Circ. Res.* **2000**, *86*, 580−588.
(57) Lerch, R.; Tamm, C.; Papageorgiou, I.; Benzi, R. H. Myocardial fatty acid oxidation during ischemia and reperfusion. *Mol. Cell. Biochem.* **1992**, *116*, 103−109.
(58) Aasum, E.; Khalid, A. M.; Gudbrandsen, O. A.; How, O. J.; Berge, R. K.; Larsen, T. S. Fenofibrate modulates cardiac and hepatic metabolism and increases ischemic tolerance in diet-induced obese mice. *J. Mol. Cell. Cardiol.* **2008**, *44*, 201−209.
(59) Bassiouni, W.; Valencia, R.; Mahmud, Z.; Seubert, J. M.; Schulz, R. Matrix metalloproteinase-2 proteolyzes mitofusin-2 and impairs mitochondrial function during myocardial ischemia-reperfusion injury. *Basic Res. Cardiol.* **2023**, *118*, 29.
(60) Chen, C. L.; Zhang, L.; Jin, Z.; Kasumov, T.; Chen, Y. R. Mitochondrial redox regulation and myocardial ischemia-reperfusion injury. *Am. J. Physiol.: Cell Physiol.* **2022**, *322*, C12−C23.
(61) Cadenas, S. ROS and redox signaling in myocardial ischemia-reperfusion injury and cardioprotection. *Free Radical Biol. Med.* **2018**, *117*, 76−89.
(62) Lopaschuk, G. D.; Ussher, J. R.; Folmes, C. D.; Jaswal, J. S.; Stanley, W. C. Myocardial fatty acid metabolism in health and disease. *Physiol. Rev.* **2010**, *90*, 207−258.
(63) Uthman, L.; Nederlof, R.; Eerbeek, O.; Baartscheer, A.; Schumacher, C.; Buchholtz, N.; Hollmann, M. W.; Coronel, R.; Weber, N. C.; Zuurbier, C. J. Delayed ischaemic contracture onset by empagliflozin associates with NHE1 inhibition and is dependent on insulin in isolated mouse hearts. *Cardiovasc. Res.* **2019**, *115*, 1533−1545.
(64) Zhang, F.; Ge, W.; Ruan, G.; Cai, X.; Guo, T. Data-independent acquisition mass spectrometry-based proteomics and software tools: A glimpse in 2020. *Proteomics* **2020**, *20*, No. e1900276.
(65) Kitata, R. B.; Yang, J. C.; Chen, Y. J. Advances in data-independent acquisition mass spectrometry towards comprehensive digital proteome landscape. *Mass Spectrom. Rev.* **2022**, *42*, 2324−2348.
(66) Olson, A. K.; Hyyti, O. M.; Cohen, G. A.; Ning, X. H.; Sadilek, M.; Isern, N.; Portman, M. A. Superior cardiac function via anaplerotic pyruvate in the immature swine heart after cardiopulmonary bypass and reperfusion. *Am. J. Physiol.: Heart Circ. Physiol.* **2008**, *295*, H2315−H2320.
(67) Nadtochiy, S. M.; Wang, Y. T.; Zhang, J.; Nehrke, K.; Schafer, X.; Welle, K.; Ghaemmaghami, S.; Munger, J.; Brookes, P. S. Potential mechanisms linking SIRT activity and hypoxic 2-hydroxyglutarate generation: no role for direct enzyme (de)acetylation. *Biochem. J.* **2017**, *474*, 2829−2839.
(68) Yu, W.; Dittenhafer-Reed, K. E.; Denu, J. M. SIRT3 protein deacetylates isocitrate dehydrogenase 2 (IDH2) and regulates mitochondrial redox status. *J. Biol. Chem.* **2012**, *287*, 14078−14086.
(69) Popova, T.; Carvalho, M. A. A. P. d.; Matasova, L.; Medvedeva, L. Regulation of mitochondrial NADP-isocitrate dehydrogenase in rat heart during ischemia. *Mol. Cell. Biochem.* **2007**, *294*, 97−105.
(70) Dean, R. A.; Overall, C. M. Proteomics discovery of metalloproteinase substrates in the cellular context by iTRAQ labeling

https://doi.org/10.1021/acs.jproteome.3c00754
J. Proteome Res. 2024, 23, 844−856

reveals a diverse MMP-2 substrate degradome. *Mol. Cell. Proteomics* **2007**, *6*, 611−623.
(71) Brown, D. A.; Perry, J. B.; Allen, M. E.; Sabbah, H. N.; Stauffer, B. L.; Shaikh, S. R.; Cleland, J. G.; Colucci, W. S.; Butler, J.; Voors, A. A.; Anker, S. D.; Pitt, B.; Pieske, B.; Filippatos, G.; Greene, S. J.; Gheorghiade, M. Expert consensus document: Mitochondrial function as a therapeutic target in heart failure. *Nat. Rev. Cardiol.* **2017**, *14*, 238−250.
(72) Gadicherla, A. K.; Stowe, D. F.; Antholine, W. E.; Yang, M.; Camara, A. K. Damage to mitochondrial complex I during cardiac ischemia reperfusion injury is reduced indirectly by anti-anginal drug ranolazine. *Biochim. Biophys. Acta* **2012**, *1817*, 419−429.
(73) Jiang, L.; Yin, X.; Chen, Y. H.; Chen, Y.; Jiang, W.; Zheng, H.; Huang, F. Q.; Liu, B.; Zhou, W.; Qi, L. W.; Li, J. Proteomic analysis reveals ginsenoside Rb1 attenuates myocardial ischemia/reperfusion injury through inhibiting ROS production from mitochondrial complex I. *Theranostics* **2021**, *11*, 1703−1720.
(74) Williams, G. S.; Boyman, L.; Lederer, W. J. Mitochondrial calcium and the regulation of metabolism in the heart. *J. Mol. Cell. Cardiol.* **2015**, *78*, 35−45.
(75) Allen, D. G.; Cairns, S. P.; Turvey, S. E.; Lee, J. A. Intracellular calcium and myocardial function during ischemia. *Adv. Exp. Med. Biol.* **1993**, *346*, 19−29.
(76) Vandecaetsbeek, I.; Raeymaekers, L.; Wuytack, F.; Vangheluwe, P. Factors controlling the activity of the SERCA2a pump in the normal and failing heart. *Biofactors* **2009**, *35*, 484−499.
(77) Stammers, A. N.; Susser, S. E.; Hamm, N. C.; Hlynsky, M. W.; Kimber, D. E.; Kehler, D. S.; Duhamel, T. A. The regulation of sarco(endo)plasmic reticulum calcium-ATPases (SERCA). *Can. J. Physiol. Pharmacol.* **2015**, *93*, 843−854.
(78) Pho, M.; Lee, W.; Watt, D. R.; Laschinger, C.; Simmons, C. A.; McCulloch, C. A. Cofilin is a marker of myofibroblast differentiation in cells from porcine aortic cardiac valves. *Am. J. Physiol.: Heart Circ. Physiol.* **2008**, *294*, H1767−H1778.
(79) Chatzifrangkeskou, M.; Yadin, D.; Marais, T.; Chardonnet, S.; Cohen-Tannoudji, M.; Mougenot, N.; Schmitt, A.; Crasto, S.; Di Pasquale, E.; Macquart, C.; Tanguy, Y.; Jebeniani, I.; Pucéat, M.; Morales Rodriguez, B.; Goldmann, W. H.; Dal Ferro, M.; Biferi, M. G.; Knaus, P.; Bonne, G.; Worman, H. J.; Muchir, A. Cofilin-1 phosphorylation catalyzed by ERK1/2 alters cardiac actin dynamics in dilated cardiomyopathy caused by lamin A/C gene mutation. *Hum. Mol. Genet.* **2018**, *27*, 3060−3078.
(80) Fagerberg, L.; Hallström, B. M.; Oksvold, P.; Kampf, C.; Djureinovic, D.; Odeberg, J.; Habuka, M.; Tahmasebpoor, S.; Danielsson, A.; Edlund, K.; Asplund, A.; Sjöstedt, E.; Lundberg, E.; Szigyarto, C. A.; Skogs, M.; Takanen, J. O.; Berling, H.; Tegel, H.; Mulder, J.; Nilsson, P.; Schwenk, J. M.; Lindskog, C.; Danielsson, F.; Mardinoglu, A.; Sivertsson, A.; von Feilitzen, K.; Forsberg, M.; Zwahlen, M.; Olsson, I.; Navani, S.; Huss, M.; Nielsen, J.; Ponten, F.; Uhlén, M. Analysis of the human tissue-specific expression by genome-wide integration of transcriptomics and antibody-based proteomics. *Mol. Cell. Proteomics* **2014**, *13*, 397−406.
(81) Subramanian, K.; Gianni, D.; Balla, C.; Assenza, G. E.; Joshi, M.; Semigran, M. J.; Macgillivray, T. E.; Van Eyk, J. E.; Agnetti, G.; Paolocci, N.; Bamburg, J. R.; Agrawal, P. B.; Del Monte, F. Cofilin-2 phosphorylation and sequestration in myocardial aggregates: novel pathogenetic mechanisms for idiopathic dilated cardiomyopathy. *J. Am. Coll. Cardiol.* **2015**, *65*, 1199−1214.
(82) McDonough, A. A.; Veiras, L. C.; Minas, J. N.; Ralph, D. L. Considerations when quantitating protein abundance by immunoblot. *Am. J. Physiol.: Cell Physiol.* **2015**, *308*, C426−C433.
(83) Ferdinandy, P.; Panas, D.; Schulz, R. Peroxynitrite contributes to spontaneous loss of cardiac efficiency in isolated working rat hearts. *Am. J. Physiol.* **1999**, *276*, H1861−H1867.
(84) Araya, L. E.; Soni, I. V.; Hardy, J. A.; Julien, O. Deorphanizing caspase-3 and caspase-9 substrates in and out of apoptosis with deep substrate profiling. *ACS Chem. Biol.* **2021**, *16*, 2280−2296.
(85) Luo, S. Y.; Moussa, E. W.; Lopez-Orozco, J.; Felix-Lopez, A.; Ishida, R.; Fayad, N.; Gomez-Cardona, E.; Wang, H.; Wilson, J. A.; Kumar, A.; Hobman, T. C.; Julien, O. Identification of human host substrates of the SARS-CoV-2 M^{pro} and PL^{pro} using subtiligase N-terminomics. *ACS Infect. Dis.* **2023**, *9*, 749−761.
(86) Chen, M.; Won, D. J.; Krajewski, S.; Gottlieb, R. A. Calpain and mitochondria in ischemia/reperfusion injury. *J. Biol. Chem.* **2002**, *277*, 29181−29186.
(87) Chelko, S. P.; Keceli, G.; Carpi, A.; Doti, N.; Agrimi, J.; Asimaki, A.; Beti, C. B.; Miyamoto, M.; Amat-Codina, N.; Bedja, D.; Wei, A. C.; Murray, B.; Tichnell, C.; Kwon, C.; Calkins, H.; James, C. A.; O'Rourke, B.; Halushka, M. K.; Melloni, E.; Saffitz, J. E.; Judge, D. P.; Ruvo, M.; Kitsis, R. N.; Andersen, P.; Di Lisa, F.; Paolocci, N. Exercise triggers CAPN1-mediated AIF truncation, inducing myocyte cell death in arrhythmogenic cardiomyopathy. *Sci. Transl. Med.* **2021**, *13*, No. eabf0891.

https://doi.org/10.1021/acs.jproteome.3c00754
J. Proteome Res. 2024, 23, 844−856